Applied Catalysis A: General 477 (2014) 132–140

Contents lists available at ScienceDirect

Applied Catalysis A: General

journal homepage: www.elsevier.com/locate/apcata

Sulfonated diatomite as heterogeneous acidic nanoporous catalyst for synthesis of 14-aryl-14-H-dibenzo[*a,j*]xanthenes under green conditions

Hossein Naeimi*, Zahra Sadat Nazifi

Department of Organic Chemistry, Faculty of Chemistry, University of Kashan, Kashan 87317, Islamic Republic of Iran

ARTICLE INFO

Article history:
Received 9 December 2013
Received in revised form 5 March 2014
Accepted 6 March 2014
Available online 15 March 2014

Keywords:
Acidic nanoporous catalyst
Diatomite-supported
β-Naphthol
Aldehydes
One-pot
Eco-friendly
Xanthene

ABSTRACT

Sulfonic acid functionalized diatomite afforded diatomite-SO_3H as an efficient heterogeneous solid acid nanoporous. The resulting immobilized catalysts have been successfully used in the synthesis of 14-aryl-14-H-dibenzo[*a,j*]xanthenes under solvent free conditions. This procedure has a lot of advantages such as very easy reaction conditions, recyclable heterogeneous acidic catalyst, natural catalyst, absence of any tedious workup or purification and much milder method. The corresponding products have been obtained in excellent yields, high purity and short reaction times.

1. Introduction

Diatomite ($SiO_2 \cdot nH_2O$) is a kind of mineral assemblage in natural sediments. It consists of frustule, the silicified hard shell of diatom [1]. The diatom shell, which is composed of amorphous silica, has properties such as high porosity with strong adsorbability and excellent thermal resistance [2]. Due to the extremely porous structure, low density and high surface area of diatomite, there is a possibility to use it for the adsorption of organic and inorganic chemicals [3]. Hence, diatomite has been widely used as alteration media, catalytic support as an adsorbent for pet litter and oil spills [4]. Although diatomite has a unique combination of physical and chemical properties, its use as an adsorbent in wastewater treatment has not been extensively investigated [5–8]. Recently, the novel applications of diatomite as biological support, pharmic carrier, chromatogram support, and functional filler have attracted extensive attentions [9,10].

Xanthene derivatives posses a broad range of useful biological and pharmacological properties such as antibacterial [11], anti-inflammatory activities [12], antiviral [13], and photodynamic therapy [14]. Furthermore, some other their derivatives have found application in industry such as dyes [15], laser technology [16], and pH sensitive fluorescent materials for visualization of biomolecules [17]. A number of methods have been developed for the synthesis of 14-H-dibenzo[*a,j*]xanthene by condensation of β-naphthol and aldehydes in the presence of *p*-toluene sulfonic acid [18], molecular iodine [19], $K_5CoW_{12}O_{40} \cdot 3H_2O$/silica-gel/MW [20], LiBr/MW [21], amberlyst-15 [22], α-iodoacetates from alkenes/ammonium acetate/I_2 [23], cation-exchange resins [24] as catalyst, Beckmann rearrangement products [25], isonitriles [26], silica sulfuric acid [27] and sulfamic acid [28].

Therefore, the synthesis of these class heterocyclic compounds is particularly significant and interest researches. Hence the synthesis of heterocycles under solvent free conditions has attracted much attention in synthetic organic chemistry.

In this research, we hope to report a simple, efficient method for the synthesis of 14-aryl-14-H-dibenzo[*a,j*]xanthenes by reaction of β-naphthol and aromatic aldehydes in the presence of diatomite-SO_3H as heterogeneous acidic catalyst. In this reaction, the catalyst

* Corresponding author. Tel.: +98 3615912388; fax: +98 3615912397.
E-mail address: naeimi@kashanu.ac.ir (H. Naeimi).

http://dx.doi.org/10.1016/j.apcata.2014.03.012
0926-860X/

could be recycled several times without significant loss of activity and high purity.

2. Experimental

2.1. Materials

All commercially available reagents were used without further purification and purchased from the Merck Chemical Company in high purity. The used solvents were purified by standard procedure.

2.2. Apparatus

IR spectra were obtained as KBr pellets on a Perkin-Elmer 781 spectrophotometer and on an impact 400 Nicolet FT-IR spectrophotometer. ^{1}H NMR and ^{13}C NMR were recorded in $CDCl_3$ solvents on a Bruker DRX-400 spectrometer with tetramethylsilane as internal reference. UV–vis spectra were obtained with a Perkin-Elmer 550 was recorded in $CDCl_3$ solvents. XRF analysis was recorded on X-ray fluorescence, Bruker, S4. Nanostructures were characterized using a Holland Philips Xpert X-ray powder diffraction (XRD) diffractometer (Cu Kα, radiation, k = 0.154056 nm), at a scanning speed of 2°/min from 10° to 100° (2Ø). Thermo gravimetric analyses (TGA) were conducted on a Rheometric Scientific Inc. 1998 thermal analysis apparatus under a N_2 atmosphere at a heating rate of 10 °C/min. Scanning electron microscope (SEM) of diatomite was performed on a FESEM Hitachi S4160. The Bandelin ultrasonic HD 3200 with probe model KE 76, 6 mm diameter, was used to produce ultrasonic irradiation and homogenizing the reaction mixture. The N_2 adsorption/desorption analysis (BET) was performed by using an automated gas adsorption analyzer (Tristar 3020, V1.03). Melting points obtained with a Yanagimoto micro melting point apparatus are uncorrected. The purity determination of the substrates and reaction monitoring were accomplished by TLC on silica-gel polygram SILG/UV 254 plates (from Merck Company).

2.3. Preparation of diatomite-SO_3H

In a typical experiment, diatomite was activated in vacuum at 100 °C and then after cooling to room temperature, diatomite (2 g) was dispersed in dry CH_2Cl_2 at room temperature under continuous stirring. After 2 h, 1 ml chlorosulfonic acid was added to the mixture of dispersion and stirred overnight. Then the solution was filtered under reduced pressure and the obtained materials thoroughly washed with dry CH_2Cl_2 then dried at 120 °C for 12 h. In this step, the modified diatomite-SO_3H was obtained as a solid acid catalyst in the organic synthesis.

2.4. A typical procedure for the synthesis of 14-aryl-14-H-dibenzo[a,j]xanthenes

A mixture of aldehyde (1 mmol), β-naphthol (2 mmol, 0.288 g) and diatomite-SO_3H (0.05 g) was heated at 90 °C under solvent free conditions at 110 °C for the appropriate time according to Table 3. The progress of the reactions was monitored by TLC (ethyl acetate/petroleum ether 3/7). After completion of the reaction, the mixture was cooled to room temperature and 10 ml CH_2Cl_2 was added. The catalyst was filtered off by simple filteration. The obtained liquid was heated by evaporation on a rotary evaporator. The obtained product was purified by recrystallization from ethanol to afford the pure products. All of the pure products were characterized by comparison of their physical and spectral data with those of authentic samples [36,32,37,38].

14-(Phenyl)14H-dibenzo[*a,j*]xanthenes (**3a**): pale yellow solid, m.p. = 183–184 °C, (m.p. = 182–183 °C) [36]; IR (KBr)/υ (cm^{-1}): 3061, 1624, 1592, 1513, 1459, 1410, 1248, 1078, 962, 805, 744; ^{1}H NMR ($CDCl_3$, 400 MHz)/δ ppm: 6.50 (s, 1H, CH), 6.98–7.01 (t, 1H, J = 7.6, Ar), 7.13–7.17 (t, 2H, J = 7.6, Ar), 7.40–7.43 (t, 2H, J = 7.6, Ar), 7.48–7.54 (m, 4H, Ar), 7.56–7.60 (t, 2H, J = 7.2, Ar), 7.81–7.92 (d, 2H, J = 8.8, Ar), 7.82–7.85 (d, 2H, J = 8.0, Ar), 8.39–8.41 (d, 2H, J = 8.8, Ar); ^{13}C NMR/($CDCl_3$, 100 MHz)/δ ppm: 148.74, 145.03, 131.48, 131.07, 128.88, 128.82, 128.5, 128.29, 126.81, 126.42, 124.26, 122.72, 118.04, 117.34, 38.07, UV (CH_2Cl_2)/λ_{max} (nm): 244, 232.

14-(4-Chlorophenyl)14H-dibenzo[*a,j*]xanthenes (**3b**): yellow solid, m.p. = 289–290 °C, (m.p. = 287–288 °C) [36]; IR (KBr)/υ (cm^{-1}): 3067, 1624, 1591, 1514, 1585, 1431, 1243, 1085, 961, 808, 743; ^{1}H NMR ($CDCl_3$, 400 MHz)/δ ppm: 6.48 (s, 1H, CH), 7.10–7.12 (d, 2H, J = 8.4, Ar), 7. 41–7.47 (m, 4H, Ar), 7.48–7.50 (d, 2H, J = 8.8, Ar), 7.57–7.61 (t, 2H, J = 7.6, Ar), 7.80–7.82 (d, 2H, J = 8.8, Ar), 7.84–7.86 (d, 2H, J = 8.0, Ar), 8.32–8.34 (d, 2H, J = 8.4, Ar); ^{13}C NMR/($CDCl_3$, 100 MHz)/δ ppm: 148.51, 145.01, 131.39, 131.31, 131.20, 130.19, 129.83, 129.19, 128.91, 127.60, 125.14, 123.77, 118.21, 117.50, 39.87; UV (CH_2Cl_2)/λ_{max} (nm): 244, 230.

14-(2-Chlorophenyl)14H-dibenzo[*a,j*]xanthenes (**3c**): white solid, m.p. = 212–213 °C, (m.p. = 214–215 °C) [36]; IR (KBr)/υ (cm^{-1}): 3059, 1625, 1591, 1462, 1402, 1243, 1032, 959, 808; ^{1}H NMR ($CDCl_3$, 400 MHz)/δ ppm: 6.81 (s, 1H, CH), 6.92 (m, 2H, Ar), 7.40–7.44 (m, 3H, Ar), 7.48–7.51 (d, 2H, J = 8.8, Ar), 7.61–7.64 (m, 5H, Ar), 8.74–8.76 (d, 2H, J = 8.4, Ar); ^{13}C NMR/($CDCl_3$, 100 MHz)/δ ppm: 148.95, 143.59, 131.83, 130.92, 130.15, 129.61, 129.06, 128.67, 127.96, 127.88, 126.94, 124.45, 123.49, 118.12, 118.02, 34.65; UV (CH_2Cl_2)/λ_{max} (nm): 246, 230.

14-(2-Nitrophenyl)14H-dibenzo[*a,j*]xanthenes (**3d**): yellow solid, m.p. = 213–214 °C, (m.p. = 214–215 °C) [36]; IR (KBr)/υ (cm^{-1}): 3057, 1625, 1591, 1500, 1395, 1346, 1305, 817, 751; ^{1}H NMR ($CDCl_3$, 400 MHz)/δ ppm: 7.08 (t, 1H, J = 8.0, CH), 7.23–7.27 (t, 1H, J = 7.2, Ar), 7.42–7.46 (t, 2H, J = 7.2, Ar), 7.42–7.49 (m, 3H, Ar), 7.57–7.63 (m, 3H, Ar), 7.81–7.84 (m, 4H, Ar), 8.53–8.55 (d, 2H, J = 8.4, Ar); ^{13}C NMR/($CDCl_3$, 100 MHz)/δ ppm: 149.4, 147.03, 140.87, 134.14, 132.26, 131.72, 130.97, 129.47, 128.73, 127.59, 127.41, 124.92, 124.67, 122.58, 118.03, 117.58; UV (CH_2Cl_2)/λ_{max} (nm): 244, 230.

14-(3-Nitrophenyl)14H-dibenzo[*a,j*]xanthenes (**3e**): yellow solid, m.p. = 212–213 °C, (m.p. = 210–211 °C) [36]; IR (KBr)/υ (cm^{-1}): 3075, 1592, 1527, 1500, 1397, 1346, 1252, 1080, 958, 812, 748; ^{1}H NMR ($CDCl_3$, 400 MHz)/δ ppm: 6.62 (s, 1H, CH), 7.28–7.32 (t, 1H, J = 7.6, Ar), 7.43–7.47 (t, 2H, J = 7.6, Ar), 7.51–7.53 (d, 2H, J = 8.8, Ar), 7.60–7.64 (t, 2H, J = 7.2, Ar), 7.81–7.87 (m, 6H, Ar), 8.30–8.32 (d, 2H, J = 8.4, Ar), 8.42 (s, 1H, Ar); ^{13}C NMR/($CDCl_3$, 100 MHz)/δ ppm: 148.77, 148.21, 146.94, 134.27, 131.04, 129.58, 129.49, 129.07, 127.25, 124.58, 122.71, 122.04, 121.69, 118.13, 115.87, 37.71; UV (CH_2Cl_2)/λ_{max} (nm): 246, 228.

14-(4-Nitrophenyl)14H-dibenzo[*a,j*]xanthenes (**3f**): pale yellow solid, m.p. = 308–309 °C, (m.p. = 310–311 °C) [36]; IR (KBr)/υ (cm^{-1}): 3068, 1593, 1516, 1341, 1245, 824, 745; ^{1}H NMR ($CDCl_3$, 400 MHz)/δ ppm: 6.61 (s, 1H, CH), 7.43–7.47 (t, 2H, Ar), 7.50–7.53 (d, 2H, Ar), 7.59–7.63 (t, 2H, Ar), 7.68–7.70 (d, 2H, Ar), 7.84–7.89 (t, 4H, Ar), 8.00–8.02 (d, 2H, Ar), 8.28–8.31 (d, 2H, Ar); ^{13}C NMR/($CDCl_3$, 100 MHz)/δ ppm: 152.01, 148.77, 146.29, 131.06, 129.6, 129.07, 128.97, 127.19, 124.60, 123.87, 122.04, 118.07, 115.76, 37.87; UV (CH_2Cl_2)/λ_{max} (nm): 248, 228.

14-(4-Chloro-3-nitrophenyl)14H-dibenzo[*a,j*]xanthenes (**3g**): yellow solid, m.p. = 232–234 °C, (m.p. = 232–234 °C) [37]; IR (KBr)/υ (cm^{-1}): 3055, 1623, 1592, 1530, 1463, 1351, 1246, 952, 811, 742; ^{1}H NMR ($CDCl_3$, 400 MHz)/δ ppm: 7.27 (s, 1H, CH), 7.29–7.31 (d, 1H, J = 8.4, Ar), 7.45–7.52 (m, 4H, Ar), 7.62–7.65 (m, 3H, Ar), 7.84–7.89 (t, 4H, J = 9.2, Ar), 8.02–8.04 (d, 1H, J = 2.0, Ar), 8.24–8.26 (d, 2H, J = 8.4, Ar); UV (CH_2Cl_2)/λ_{max} (nm): 246, 232.

14-(2,4-Dichlorophenyl)14H-dibenzo[*a,j*]xanthenes (**3h**): pale yellow solid, m.p. = 229–230 °C, (m.p. = 227–228 °C) [36]; IR (KBr)/υ (cm^{-1}): 3060, 1622, 1590, 1514, 1464, 1430, 1401, 1247, 1103, 1072, 960, 864, 836, 807, 743; ^{1}H NMR ($CDCl_3$, 400 MHz)/δ ppm:

6.77 (s, 1H, CH), 6.90–6.92 (d, 1H, Ar), 7.28–7.33 (m, 2H, Ar), 7.43–7.50 (m, 4H, Ar), 7.61–7.65 (t, 2H, J = 7.6, Ar), 7.81–7.85 (t, 4H, J = 9.0, Ar), 8.65–8.67 (d, 2H, J = 8.0, Ar); ^{13}C NMR/($CDCl_3$, 100 MHz)/δ ppm: 148.9, 142.25, 132.8, 132.71, 132.6, 130.92, 130.59, 129. 4, 128.78, 128.41, 127.06, 124.57, 123.17, 118.11, 117.46, 34.24; UV (CH_2Cl_2)/λ_{max} (nm): 248, 230.

14-(2,3-Dichlorophenyl)14H-dibenzo[*a,j*]xanthenes (**3i**): white solid, m.p. = 251–253 °C, (m.p. = 250–253 °C) [37]; IR (KBr)/υ (cm^{-1}): 3057, 1625, 1593, 1515, 1459, 1405, 1401, 1252, 1107, 1070, 962, 869, 813, 807, 746; ^{1}H NMR ($CDCl_3$, 400 MHz)/δ ppm: 6.85 (s, 1H, CH), 6.87–6.89 (d, 1H, J = 8.0, Ar); 7.09–7.11 (d, 2H, J = 8.8, Ar), 7.32–7.34 (d, 1H, J = 9.2, Ar), 7.44–7.51 (m, 4H, Ar), 7.62–7.85 (t, 4H, J = 9.2, Ar), 8.69–8.67 (d, 2H, J = 8.4, Ar); UV (CH_2Cl_2)/λ_{max} (nm): 248, 231.

14-(3-Hydroxyphenyl)14H-dibenzo[*a,j*]xanthenes (**3j**): Pale Pink solid, m.p. = 172–173 °C, (m.p. = 174–176 °C) [38]; IR (KBr)/υ (cm^{-1}): 3068, 1593, 1513, 1402, 1251, 1242, 810; ^{1}H NMR ($CDCl_3$, 400 MHz)/δ ppm: 3.58 (s, 3H), 6.42 (s, 1H), 6.47 (d, 1H, J = 8.2 Hz), 7.05 (t, 2H, J = 8.4 Hz), 7.13 (d, 1H, J = 7.5 Hz), 7.39 (t, 2H, J = 7.2 Hz), 7.43 (d, 2H, J = 9.0 Hz), 7.53 (t, 2H, J = 7.6 Hz), 7.72–7.82 (m, 4H), 8.36 (d, 2H, J = 8.7 Hz).

14-(4-Hydroxyphenyl)14H-dibenzo[*a,j*]xanthenes (**3k**): Pink solid, m.p. = 137–138 °C, (m.p. = 138–140 °C) [38]; IR (KBr)/υ (cm^{-1}): 3405, 1592, 1511, 1402, 1250, 1242, 815; ^{1}H NMR ($CDCl_3$, 400 MHz)/δ ppm:4.97 (br s, 1H, OH), 6.43(s, 1H, CH), 6.55–8.36 (m, 16H, Ar); ^{13}C NMR/($CDCl_3$, 100 MHz)/δ ppm: 37.41, 115.70, 118.00, 118.40, 123.10, 124.62, 127.23, 129.11, 129.20, 129.78, 131.53, 131.81, 137.90, 149.11, 154.24.

14-(3-Methoxy)14H-dibenzo[*a,j*]xanthenes (**3l**): Pale pink solid, m.p. = 173–174 °C, (m.p. = 174–176 °C) [36]; IR (KBr)/υ (cm^{-1}): 3067, 3014, 2934, 1582, 1454, 1431, 1401, 1247, 1050, 964, 806, 743; ^{1}H NMR ($CDCl_3$, 400 MHz)/δ ppm:3.63 (s, 3H, OCH_3), 6.45 (s, 1H, CH), 6.51 (dd, 2H, J = 7.5 Hz, ArH), 7.02–7.46 (m, 6H, ArH), 7.55 (t, 2H, J = 7.5 Hz, ArH), 7.78 (t, 4H, J = 7.5 Hz, ArH), 8.39 (d, 2H, J = 7.5 Hz, ArH) ppm.

14-(4-Methoxy)14H-dibenzo[*a,j*]xanthenes (**3 m**): pink solid, m.p. = 204–205 °C, (m.p. = 202–203 °C) [39], IR (KBr)/υ (cm^{-1}): 3062, 1594, 1510, 1458, 1398, 1248, 960, 814, 744; ^{1}H NMR ($CDCl_3$, 400 MHz)/δ ppm: 6.45 (s, 1H, CH), 6.67–6.69 (d, 2H, J = 8.4, Ar), 7.40–7.44 (m, 4H, Ar), 7.47–7.49 (d, 2H, J = 8.8, Ar), 7.56–7.60 (t, 2H, J = 7.2, Ar), 7.78–7.80 (d, 2H, J = 8.8, Ar), 7.82–8.84 (d, 2H, J = 8.0, Ar), 8.38–8.40 (d, 2H, J = 8.4, Ar); ^{13}C NMR/($CDCl_3$, 100)/δ ppm: 37.14, 55.06, 113.87, 117.55, 118.04, 122.73, 123.60, 124.25, 126.40, 126.79, 128.77, 128.84, 129.20, 131.11, 131.45, 137.42, 148.68, 157.86; UV (CH_2Cl_2)/λ_{max} (nm): 246, 230.

14-(4-Methyl)14H-dibenzo[*a,j*]xanthenes (**3n**): pale yellow solid, m.p. = 228–230 °C, (m.p. = 227–228 °C) [36], IR (KBr)/υ (cm^{-1}): 3069, 1623, 1591, 1531, 1458, 1399, 1244, 961, 810, 741; ^{1}H NMR ($CDCl_3$, 400 MHz)/δ ppm: 6.46 (s, 1H, CH), 6.95–6.97 (d, 2H, J = 8.0, Ar), 7.39–7.43 (m, 4H, Ar), 7.47–7.50 (d, 2H, J = 9.2, Ar), 7.56–7.60 (t, 2H, J = 9.2, Ar), 7.78–7.80 (d, 2H, J = 8.8, Ar), 7.82–8.84 (d, 2H, J = 8.0, Ar), 8.39–8.41 (d, 2H, J = 8.8, Ar); ^{13}C NMR/($CDCl_3$, 100)/δ ppm: 20.91, 37.64, 117.46, 118.02, 122.72, 124.22, 126.77, 128.11, 128.77, 128.79, 129.19, 131.08, 131.46, 135.91, 142.14, 148.68; UV (CH_2Cl_2)/λ_{max} (nm): 247, 232.

3. Results and discussion

3.1. Characterization of diatomite-SO_3H

Diatomite is a type of widespread natural nanoporous material which provides a suitable support. A new heterogeneous catalyst has been prepared from the reaction of diatomite and chlorosulfonic acid (Scheme 1).

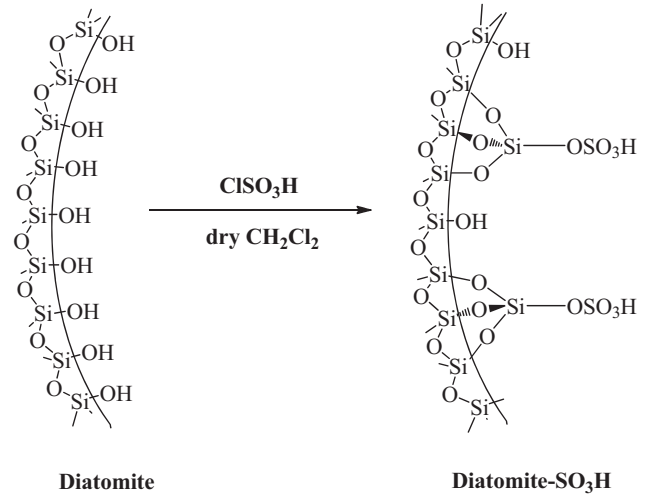

Scheme 1. Preparation of diatomite-SO_3H.

The functional groups attached to diatomite are quantitatively determined by back acid–base titration (−SO_3H) in diatomite-SO_3H 0.2 mmol H^+ sites per 0.02 g of diatomite-SO_3H (values calculated by the weight of diatomite-SO_3H) at 25 °C. Also, the pH of resulted diatomite-SO_3H (10%, w/v) was determined using pH meter. At first 0.5 g diatomite-SO_3H was dispersed in 5 ml H_2O by ultrasonic bath for 60 min then measured and approximately about 0.48.

The XRF of Bardscan diatomite and diatomite-SO_3H were provided and the results are indicated below: The parent material, had the following chemical composition (in mass%): SiO_2 (66.39), Al_2O_3 (11.30), Fe_2O_3 (4.30), CaO (3.42), MgO (1.62), BaO (3.06), SO_3 (3.02), K_2O (1.11), Na_2O (0.905), TiO_2 (0.431), P_2O_5 (0.230), SrO (0.222), MnO (0.085), Cl (0.03), ZrO_2 (0.025), Cr_2O_3 (0.018), CuO (0.017), Rb_2O (0.005) and diatomite-SO_3H had the following chemical composition (in mass%): SiO_2 (51.54), SO_3 (11.90), Al_2O_3 (8.77), BaO (3.88), Fe_2O_3 (3.59), CaO (2.94), MgO (1.14), K_2O (0.982), Na_2O (0.849), TiO_2 (0.371), SrO (0.194), Cl (0.120), P_2O_5 (0.086), MnO (0.074), Cr_2O_3 (0.024), ZrO_2 (0.019), CuO (0.018), and Rb_2O (0.005).

Scanning electron micrographs were recorded to understand morphological changes occurring on the catalyst. The SEM image of diatomite-SO_3H before and after $ClSO_3H$ treatment is shown in Fig. 1. The morphology, as observed by SEM images, shows significant difference between diatomite and diatomite-SO_3H. Diatomite had lamellar aggregates of irregular plate-like shapes which are very smooth with fluffy appearance. After sulfonation of the diatomite, the aggregates were foliated with rougher surfaces. On the other hand, it is observed that some impurities have been deposited on the diatomite particles.

The surface area (BET), pore volume and pore size of diatomite and diatomite-SO_3H were provided. The corresponding results are shown in Table 1.

The pore size distribution, as calculated by the BJH method from the desorption branch of the nitrogen isotherm, reveals that the prepared samples contain pore size between 2 and 120 nm (Fig. 2).

Table 1
Surface area, pore volume and pore size of diatomite and diatomite-SO_3H.

Name	Surface area[a] (m^2/g)	Total pore Volume (cm^3/g)	Pore size (nm)[b]
Diatomite	73.36	0.141	6.87
Diatomite-SO_3H	74.03	0.158	7.6

[a] The BET (Brunauer–Emmet–Teller) surface area.
[b] The average pore diameter was obtained by using the BJH (Barrett, Joyner and Halenda) model.

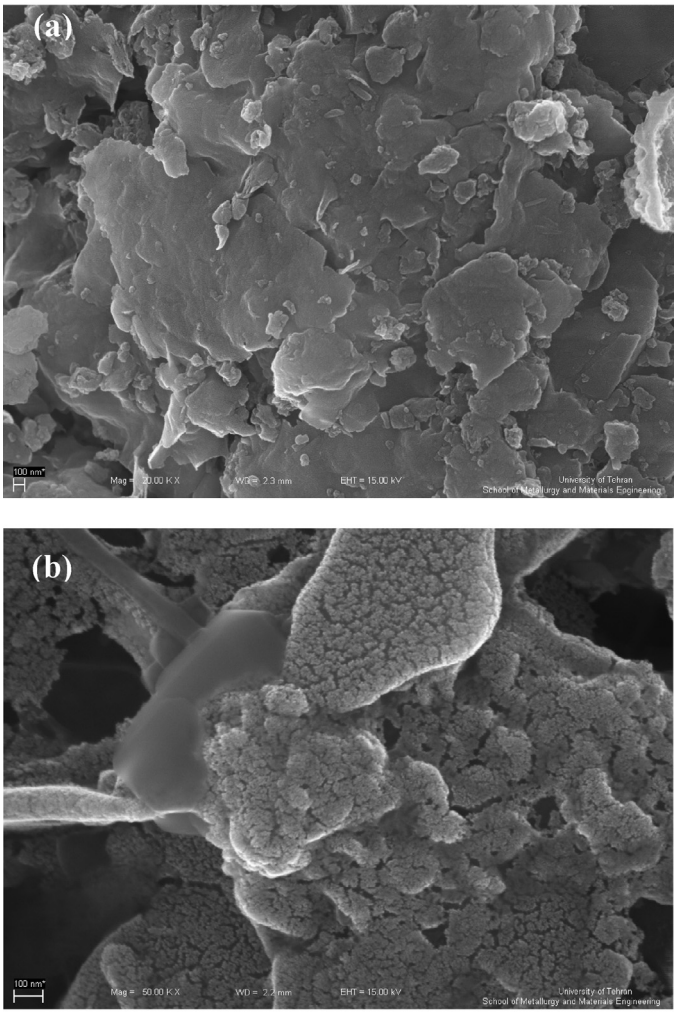

Fig. 1. SEM images of (a) diatomite (b) diatomite-SO_3H.

As shown in Fig. 3, the nitrogen adsorption/desorption isotherm of diatomite and diatomite-SO_3H was characterized as a type II isotherm with an H_3 hysteresis loop, according to the IUPAC classification [40,41]. The hysteresis is associated with the filling and emptying of the mesopores by capillary condensation. Sulfonation of diatomite did not evidently change the shape of the isotherms of the samples (Fig. 3).

A thermo gravimetric analysis (TGA) was used to study the thermal stability of the acid catalyst (Fig. 4). The TGA curve was divided into several regions corresponding to different mass lose ranges. The first region, which occurred below 150 °C, displayed a mass loss that was attributable to the loss of adsorbed solvent or trapped water from the catalyst. A weight loss of approximately 10% weight occurred between 150 and 500 °C that was likely a consequence of the loss of SO_3H groups.

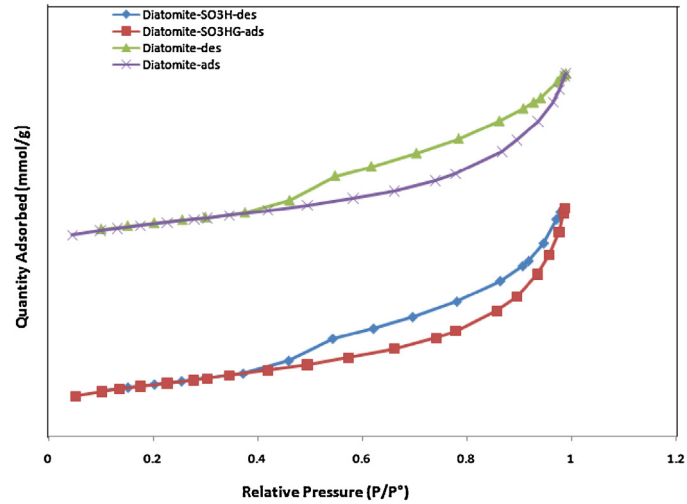

Fig. 3. Nitrogen adsorption–desorption isotherms of diatomite and diatomite-SO_3H.

The characterization of diatomite-SO_3H was performed by Fourier transform spectroscopy (FT-IR). As shown in Fig. 5, the high symmetry presented on diatomite, very weak infrared signals, due to the weak difference of charge state and very small induced electric dipole. After functionalization of diatomite, new bands are clearly seen. The presence of the sulfonic acid group is also demonstrated by the bands at 1071, 1175 and 579 cm^{-1}, which correspond to the symmetric, asymmetric SO_2 and C—S stretching modes, respectively (Fig. 5).

XRD measurement was used to identify the crystalline structure of the products. As can be shown, the XRD patterns of diatomite and diatomite-SO_3H samples are plotted in Fig. 6 can match well with the characteristic peaks, which indicate that the structure of diatomite can be remained after the surface modification with chlorosulfonic acid. The XRD patterns of the particles show characteristic peaks at (2θ = 20.0768, 22.17, 23.00, 23.82, 26.11, 26.80, 27.94, 29.01, 31.77, 33.03, 39.67, 41.07, 43.17, 49.38, 55.14, 60.43, 62.21, 65.86, 68.02, 68.02, 73.11, 75.56). The average crystallite size was calculated equal to 40.3 nm using Debye–Scherrer equation, $D = k\lambda/\beta\cos\theta$ where k is a constant (generally considered as 0.94), λ is the wavelength of Cu Kα (1.54 Å), β is the corrected diffraction line full-width at half-maximum (FWHM), and θ is Bragg's angle [35].

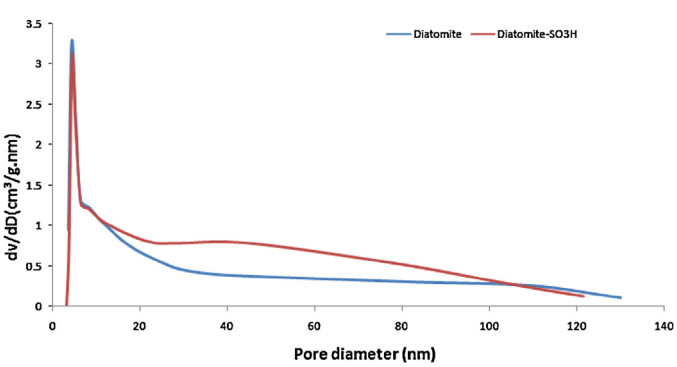

Fig. 2. Pore size distributions of diatomite and diatomite-SO_3H.

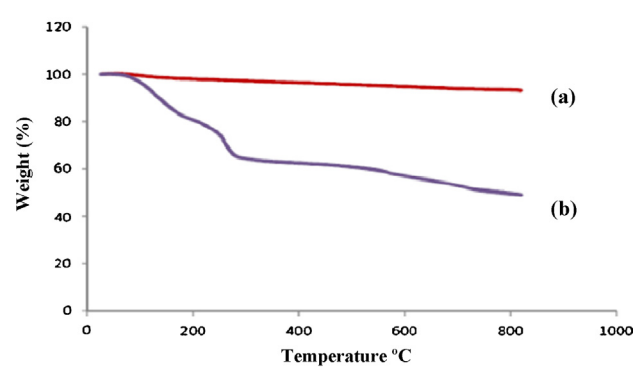

Fig. 4. TGA curves of (a) diatomite and (b) diatomite-SO_3H.

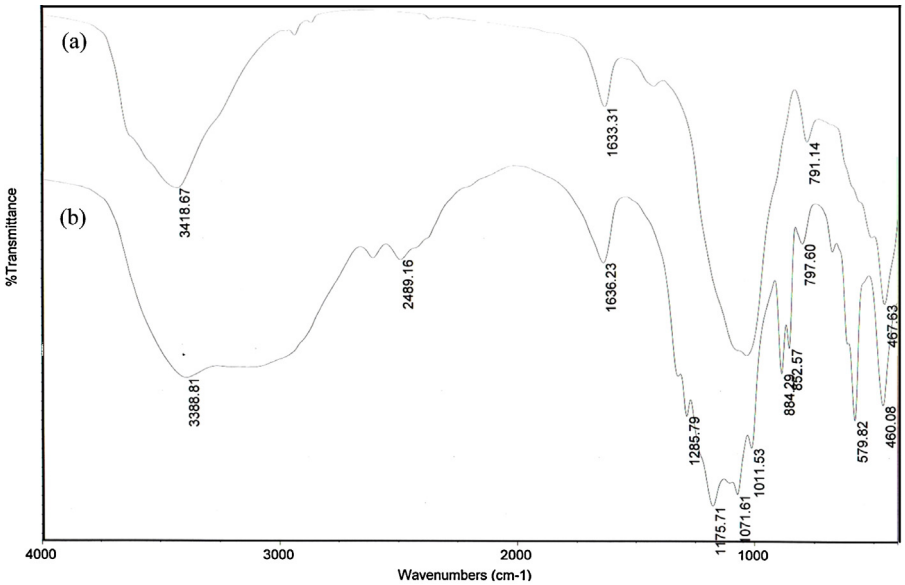

Fig. 5. FT-IR spectra of (a) diatomite and (b) diatomite-SO_3H.

3.2. Application of diatomite-SO_3H as heterogeneous catalyst in the synthesis of 14-aryl-14H-dibenzo[a,j]xanthenes

Initially, in order to optimization of the reaction conditions, we are considered the reaction of β-naphthol and 4-chlorobezaldehyde in a 2:1 ratio as a model substrate in the presence of various catalytic amounts of diatomite-SO_3H under solvent free conditions at 90 °C as a heterogeneous catalyst (Table 2). The obtained results from the reaction to determine the optimum amount of catalyst are presented in Table 2. In this reaction, the best results were obtained using 0.05 g of catalyst (as can be seen from Table 2, entry 6). While a higher amount of catalyst did not affect on desired product yield (Table 2, entry 7).

After optimization of the reaction conditions, the reaction of β-naphthol with several aldehydes was carried out according to the general experimental procedure. The corresponding products are summarized in Table 3. The yields of most xanthene products are higher than 90%. Thus, benzaldehydes bearing 4-substituents (entries 3 and 8) slightly afford the better product yields. This slight difference is also seen in 2-substituted benzaldehydes (entries 2, 4, 5 and 6). In this study, 14-aryl-14-H-dibenzo[*a,j*]xanthenes as products in a new method were prepared using the model reaction of β-naphthole and various aromatic aldehyhes in the presence of catalytic amount of diatomite-SO_3H (0.05 g) at 90 °C under solvent free conditions. After the separation of the product, the catalyst as a by-product is removable by washing with CH_2Cl_2, and easily recycled to catalyze the preparation of 14-aryl-14-H-dibenzo[*a,j*]xanthenes with excellent yields.

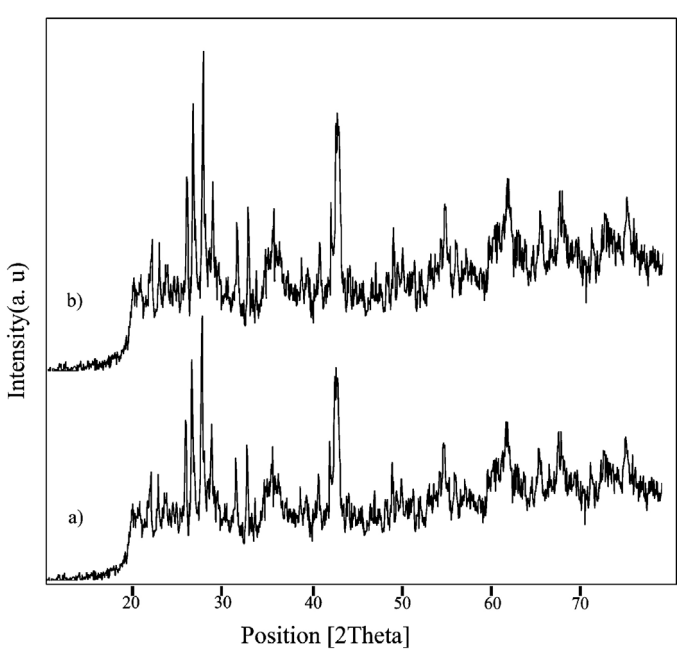

Fig. 6. XRD patterns of (a) diatomite and (b) diatomite-SO_3H.

To show the merit of the present work in comparison with reported results in the literature, we compared the results of ditomite-SO_3H catalyst with reported catalysts in the synthesis of 14-aryl-14-H-dibenzo[*a,j*]xanthenes from the reaction of β-naphthol and various aromatic aldehydes (Table 4). As can be seen in this table, the present catalyst was found to be the most efficient catalyst among all of the tested catalysts in this reaction. Though each of the above mentioned methods has demonstrated its own merits, several of these methods suffer from one or more drawbacks such as; long reaction times (Table 4, entries 2–11), use of hazardous catalyst, harsh reaction conditions, excess of catalysts and low yields (Table 4, entries 6, 8, and 11). While, the reaction in the presence of ditomite-SO_3H was indicated a lot of significant such as; low reaction times, excellent product yields, simplicity of the reaction, naturally safe, economical, eco-friendly and recyclable biomimetic catalyst. These advantages can be related to the highly activity due to its nanoporosity and high surface area.

For reusability of the catalyst, after the separation of solid products (**3f**) with CH_2Cl_2 completely, diatomite-SO_3H catalyst was recycled for several times without any decrease in catalytic activity, the yields ranged from 97% to 92% (Fig. 7).

The structure of products were confirmed by spectroscopic and physical data such as; IR, ^{1}H NMR, ^{13}C NMR and UV–vis. The infrared spectra of the 14-(4-chlorophenyl)14H-dibenzo [*a,j*]xanthene exhibit a band at 1243 cm^{-1} assigned to υ (C—O). In the ^{1}H NMR spectra the signal around δ = 7.10–8.34 ppm is assigned to the protons of the aromatic rings υ (CH=CH), the signal of the aliphatic rings υ (CH) is showed at 6.48 ppm and the ^{13}C NMR

Table 2
The synthesis of 14-(4-chlorophenyl)14H-dibenzo[*a,j*] xanthenes under different amounts of catalyst.

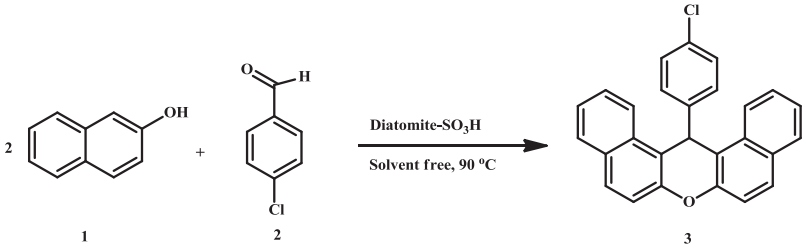

Entry	Diatomite-SO_3H (g)	Time (min)	Yield[a] (%)
1	–	180	0
2	0.02	30	20
3	0.03	30	50
4	0.04	30	75
5	0.05	30	95
6	0.05	7	95
7	0.06	30	95

[a] Isolated yields.

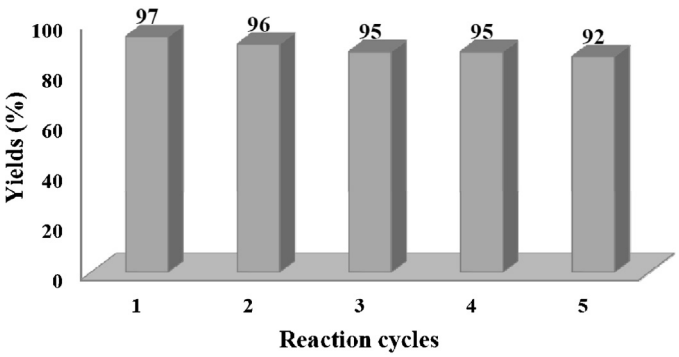

Fig. 7. Reusability of diatomite-SO_3H.

spectrum the signal around $\delta = 117.50–148.51$ ppm is assigned to the carbons of the aromatic rings (CH=CH) and the signal of the aliphatic rings υ (CH) is shown at 39.87 ppm.

3.3. The proposed reaction mechanism

The formation of 14-aryl-14-H-dibenzo[*a,j*]xanthenes from β-naphthol and aromatic aldehyde in the presence of ditomite-SO_3H as catalyst can be explained by a tentative mechanism is presented in Scheme 2. One molecule of β-naphthol was firstly condensed with an activated aromatic aldehyde (I) to provide intermediate (II), which can be regarded as a fast Knoevenagel addition. Then the active methylene of the second molecule of β-naphthol reacted with intermediate (II) via conjugate Michael addition to produce the intermediate (III), which undergoes intramolecular cyclodehydration to give the 14-aryl-14-H-dibenzo[*a,j*]xanthenes (V).

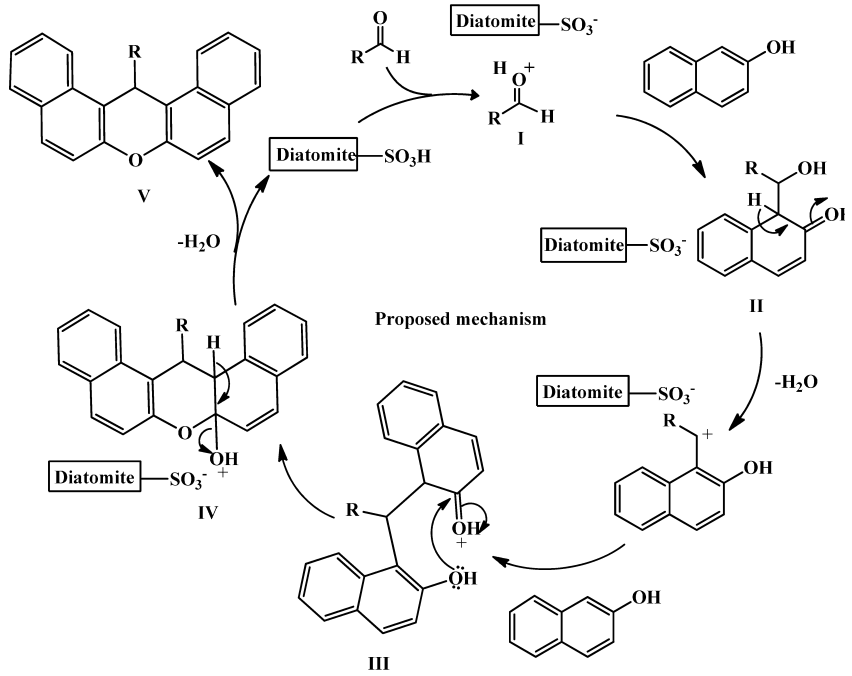

Scheme 2. Proposed reaction mechanism.

Table 3
Synthesis of 14-aryl-14-H-dibenzo[*a,j*]xanthenes in the presence of diatomite-SO_3H under solvent free conditions at 90 °C.

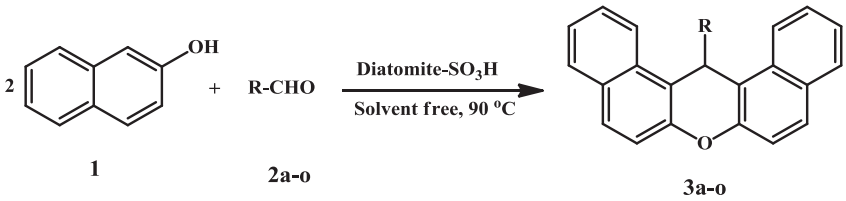

Entry	Aldehyde	Product	Time (min)	Yield[a]	TON[b]	TOF[c] (h^{-1})	M.p. (°C)	M.p. (°C)
1	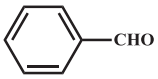	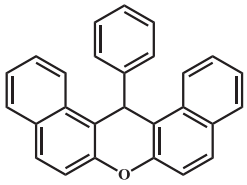	10	93	46.5	279.1	183–184	182–183
2	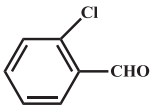	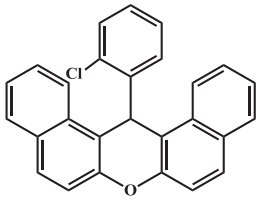	12	88	44.0	220.0	212–213	214–215
3	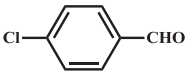	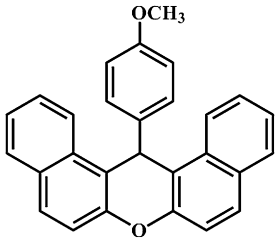	7	95	47.5	407.2	289–290	287–288
4	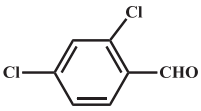	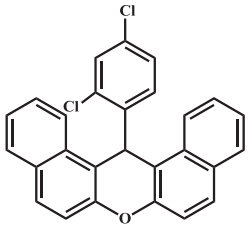	10	91	45.5	273.1	229–230	227–228
5	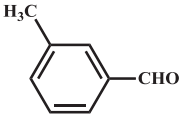	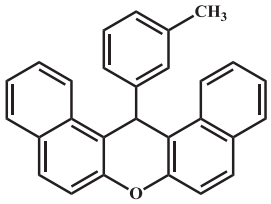	8	92	46.0	345.1	251–253	250–253
6	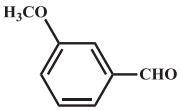	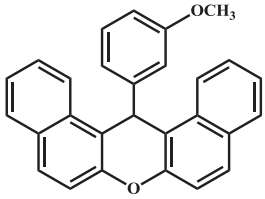	8	90	45.0	337.6	213–214	214–215
7	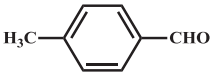	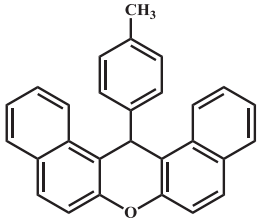	3	96	48.0	960.0	212–213	210–211

Table 3 (*Continued*)

Entry	Aldehyde	Product	Time (min)	Yield[a]	TON[b]	TOF[c] (h^{-1})	M.p. (°C)	M.p. (°C)
8	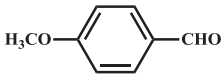	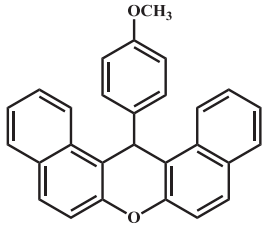	2	97	48.5	1455.2	308–309	310–311
9	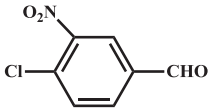	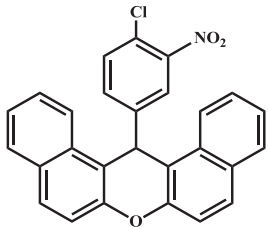	3	96	48.0	960.0	232–234	232–234
10	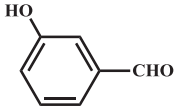	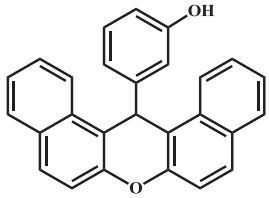	20	92	46.0	138.0	240–241	242–243
11	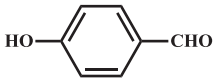	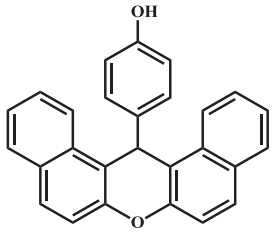	15	82	41.0	164.0	138–140	139–140
12	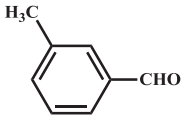	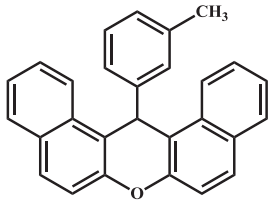	5	89	44.5	534.0	197–199	198
13	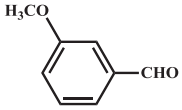	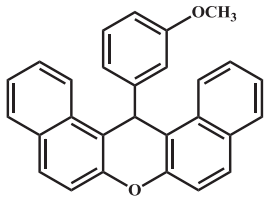	10	85	42.5	318.8	172–173	174–176
14	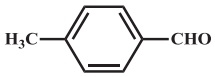	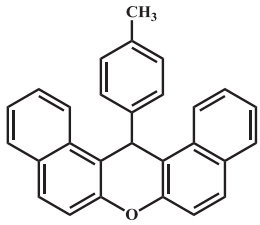	17	85	42.5	150.0	228–230	227–228

Table 3 (*Continued*)

Entry	Aldehyde	Product	Time (min)	Yield[a]	TON[b]	TOF[c] (h^{-1})	M.p. (°C)	M.p. (°C)
15	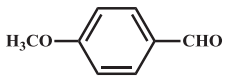	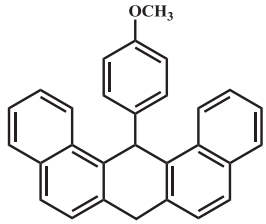	13	84	42.0	193.9	203–205	202–203

[a] Isolated yields.
[b] Turnover number represents the average number of substrate molecules converted into the product per molecule of catalyst.
[c] Turnover number per hour (TOF).

Table 4
The synthesis of 14-(4-nitrophenyl)14H-dibenzo[*a,j*]xanthene using different catalysts.

Entry	Catalyst	Time	Yield[a] (%)	Temperature (°C)	Reference
1	Diatomite-SO_3H	2 min	97	90	–
2	Cellulose sulfuric acid	120 min	90	110	[29]
3	PFPAT	180 min	96	r.t.	[30]
4	SBA-15-SO_3H	24 h	91	85	[31]
5	SiO_2-Pr-SO_3H	40 min	98	125	[32]
6	TCCA	50 min	74	110	[33]
7	H_2SO_4/SiO_2	60 min	97	125	[34]
8	Dowex-50 W	2 h	84	100	[22]
9	$Yb(OTf)_3$	3 h	91	110	[42]
10	$H_5PW_{10}V_2O_{40}$	1 h	92	100	[13]
11	Iodine	2.5 h	85	90	[43]

[a] Isolated yields.

4. Conclusions

In summary, a heterogeneous diatomite-SO_3H was prepared and characterized by XRF, BET, SEM, TGA, XRD and IR spectroscopy. In this research, we have been described the synthesis of 14-aryl-14-H-dibenzo[*a,j*]xanthenes via condensation of β-naphthol with different kinds of aromatic aldehydes. The application of diatomite-SO_3H as a highly efficient, inexpensive, easy work-up, and reusable natural catalyst makes the present procedure eco-friendly and economically acceptable. In addition, low-cost, solvent free, non-toxicity, high yields of the desired products and short reaction times is supporting the method toward the green chemistry.

Acknowledgement

The authors are grateful to University of Kashan for supporting this work by Grant No. 159148/30.

References

[1] F.Y. Wang, H.F. Zhang, Chinese J. Geochem. 14 (1995) 140–152.
[2] P. Yuana, D.Q. Wua, H.P. Hea, Z.Y. Linb, Appl. Surf. Sci. 227 (2004) 30–39.
[3] B. Bahramian, F. Doulati Ardejanib, V. Mirkhanic, K. Badiid, Appl. Catal. A: Gen. 345 (2008) 97–103.
[4] J.F. Lemonas, Am. Ceram. Soc. Bull. 6 (1997) 92–95.
[5] O. San, R. Goren, C. Ozgur, Int. J. Miner. Process. 93 (2009) 6–10.
[6] S. Aytas, S. Akyil, M.A.A. Aslani, U. Aytekin, J. Radioanal. Nucl. Chem. 240 (1999) 973–996.
[7] P.B. Michell, K. Atkinson, Miner. Eng. 4 (1991) 1091–1113.
[8] P. Yuana, D.Q. Wua, H.P. Hea, Z.Y. Lin, Appl. Surf. Sci. 227 (2004) 30–39.
[9] H. Hadjar, B. Hamdi, M. Jaber, J. Brendlé, Z. Kessaissia, H. Balard, J.B. Donnet, Microporous Mesoporous Mater. 107 (2008) 219–226.
[10] X. Li, C. Bian, W. Chen, J. He, Appl. Surf. Sci. 207 (2003) 378–383.
[11] A.N. Dadhania, V.K. Patel, D.K. Raval, C. R. Chim. 15 (2012) 378–383.
[12] J.P. Poupelin, G. Saint-Ruf, O. Foussard-Blanpin, G. Narcisse, G. Uchida-Ernouf, R. Lacroix, Eur. J. Med. Chem. 13 (1978) 67–71.
[13] R. Tayebee, S. Tizabi, Chinese J. Catal. 33 (2012) 962–969.
[14] R.M. Ion, D. Frackowiak, A. Planner, K. Wiktorowicz, Acta Biochim. Pol. 45 (1998) 833–845.
[15] A. Banerjee, A.K. Mukherjee, Stain Technol. 56 (1981) 83–85.
[16] M. Ahmad, T.A. King, D. Ko, B.H. Cha, J. Lee, J. Phys. D: Appl. Phys. 35 (2002) 1473–1476.
[17] C.G. Knight, T. Stephens, Biochem. J. 258 (1989) 683–689.
[18] A.R. Khosropour, M.M. Khodaei, H. Moghannian, Synlett (2005) 955–958.
[19] B. Das, B. Ravikanth, R. Ramu, K. Laxminarayana, B. Vittal Rao, J. Mol. Catal. A: Chem. 255 (2006) 74–77.
[20] L. Nagarapu, S. Kantevari, V.C. Mahankhali, Catal. Commun. 8 (2007) 1173–1177.
[21] A. Saini, S. Kumar, J.S. Sandhu, Synlett (2006) 1928–1932.
[22] S. Ko, C.F. Yao, Tetrahedron Lett. 47 (2006) 8827–8829.
[23] Y.Y. Myint, M.A. Pasha, Synth. Commun. 34 (2004) 4477–4482.
[24] S.B. Patil, R.P. Bhat, S.D. Samant, Synth. Commun. 36 (2006) 2163–2168.
[25] L. De Luca, G. Giacomelli, A. Porcheddu, J. Org. Chem. 67 (2002) 6272–6274.
[26] A. Porcheddu, G. Giacomelli, M. Salaris, J. Org. Chem. 70 (2005) 2163–2361.
[27] H.R. Shaterian, M. Ghashang, A. Hassankhani, Dyes Pigment 76 (2008) 564–568.
[28] B. Rajitha, B. Sunil Kumar, Y. Thirupathi Reddy, P. Narsimha Reddy, N. Sreenivasulu, Tetrahedron Lett. 46 (2005) 8691–8693.
[29] J. Venu Madhava, Y. Thirupathi Reddy, P. Narsimha Reddy, M. Nikhil Reddy, S. Kuarma, P.A. Crooksb, B. Rajitha, J. Mol. Catal. A: Chem. 304 (2009) 85–87.
[30] S. Khaksar, N. Behzadi, Chinese J. Catal. 33 (2012) 982–985.
[31] M.A. Naik, D. Sachdev, A. Dubey, Catal. Commun. 11 (2010) 1148–1153.
[32] G. Mohammadi Ziarani, A.R. Badiei, M. Azizi, Sci. Iran. C 18 (2011) 453–457.
[33] B. Maleki, M. Gholizadeh, Z. Sepehr, Bull. Korean Chem. Soc. 32 (5) (2011) 1697–1702.
[34] G.B. Dharma Rao, M.P. Kaushik, A.K. Halve, Tetrahedron Lett. 53 (2012) 2741–2744.
[35] R. Massart, IEEE Trans. Magn. 17 (1981) 1247–1248.
[36] R. Kumar, G.C. Nandi, R.K. Verma, M.S. Singh, Tetrahedron Lett. 51 (2010) 442–445.
[37] H. Naeimi, Z.S. Nazifi, J. Chinese Chem. Soc. 60 (2013) 1113–1117.
[38] S. Puri1, B. Kaur, A. Parmar, H. Kumar, Heterocyclic Lett. 1 (2011) 269–274.
[39] R. Fareghi-Alamdari, M. Golestanzadeh, F. Agend, N. Zekri, C. R. Chim. 16 (2013) 878–887.
[40] F. Meshkani, M. Rezaei, Powder Technol. 199 (2010) 144–148.
[41] G. Leofanti, M. Padovanb, G. Tozzolac, B. Venturelli, Catal. Today 41 (1998) 207–219.
[42] W. Su, D. Yang, C. Jin, B. Zhang, Tetrahedron Lett. 49 (2008) 3391–3394.
[43] G.H. Mahdavinia, S. Rostamizadeh, A.M. Amani, Z. Emdadi, Ultrason. Sonochem. 16 (2009) 7–10.